Macromolecules
ARTICLE

Macromolecules **2010**, *43*, 3521–3531 **3521**
DOI: 10.1021/ma902860j

Kinetics of Diblock Copolymer Micellization by Dissipative Particle Dynamics

Zhenlong Li and Elena E. Dormidontova*

Department of Macromolecular Science and Engineering, Case Western Reserve University, Cleveland, Ohio 44106

Received December 29, 2009; Revised Manuscript Received March 1, 2010

ABSTRACT: Micelle formation from a solution of randomly dispersed diblock copolymers in a selective solvent is found to be a three-stage process with a substantial contribution from kinetic processes involving small aggregates (dimers, trimers, etc.) and micelle fusion/fission resulting in a bimodal aggregation number distribution at intermediate times. Dissipative particle dynamics simulations were applied to study micellization kinetics and equilibrium properties of micelle solutions. The critical micelle concentration, micelle aggregation number distribution, and micelle structure were found to agree well with previous experimental and theoretical studies. The time-evolution of micelles from unimers is found to follow three stages: unimer consumption, equilibration of the number of micelles driven by the fusion/fission mechanism, and slow adjustment of the weight-average aggregation number by micelle fusion, unimer and small aggregate exchange. The effect of polymer concentration, hydrophobic interaction energy, and block length on the kinetics of micellization are also considered.

Introduction

The micellization kinetics of diblock copolymer solutions have been actively studied during the past decade, with a noticeable increase in the number of publications in recent years. This interest is due to the fundamental importance of micellization kinetics to understanding polymer self-assembly and various industrial applications, such as dispersant technology and controlled drug release.[1] Various experimental techniques, such as nonradiative energy transfer and fluorescence-quenching techniques, time-resolved light, small angle neutron and synchrotron X-ray scattering or stopped-flow have been applied to study the process of micelle formation or re-equilibration induced by sudden change in temperature (*T*-jump), pH, or solvent.[2−13] Despite numerous reports, a complete understanding of micellization kinetics, including the mechanism(s) of micelle growth and the effect of various kinetic-controlling factors, is still lacking. In this paper we apply the dissipative particle dynamics (DPD) technique to model the process of spherical micelle formation from a solution of short diblock copolymers and analyze the contribution of different processes, such as unimer exchange, micelle fusion/fission, etc. on micellization kinetics as a function of different factors (oligomer concentration, interaction energy, and block length).

Diblock copolymer micellization is a heterogeneous process, which occurs on a different time scales, varying from nanoseconds to milliseconds for the initial stages of micelle formation to hours, days, or even years for the final stage of micelle equilibration and strongly depends on the system composition, block length, solvent quality and method of induction of the micellization process. This creates several experimental challenges for the investigation of the micellization kinetics. First, real-time detection of the micellization process, especially the very early stage, is limited by the spatial and temporal resolution of current scattering techniques. Often the signal strength is insufficient to detect either individual unimers, or small aggregates, such that only reasonably large micelles can be monitored. Honda and coworkers[4] have studied the relaxation kinetics of micellization of a block copolymer solution induced by a *T*-jump by monitoring the time evolution of the apparent molecular weight and radius of gyration. The corresponding time constant associated with the average molecular weight growth has been found to decrease with an increase of polymer concentration. Micellization depends strongly on the experimental conditions, such that it is often difficult to compare the results obtained using different measurement techniques or methodologies for the induction of micellization. In a series of rapid micromixing homogeneous precipitation experiments Johnson and co-workers[6] found that the mechanism of block copolymer self-assembly depends on the rate and magnitude of the solvent quality change. They showed that using high supersaturation for a low critical micelle concentration produced frozen micelles, with the characteristic micellization time decreasing with an increase of concentration, which is consistent with the micelle fusion mechanism of micellization. On the other hand, under the conditions of a slow solvent quality change, both unimer exchange and micelle fusion take place during the micellization process. Liu and co-workers studied diblock copolymer micellization kinetics induced by a pH-jump[7,9,10] or solvent-jump.[11,12] Time-dependent light scattering has been used to probe the pH-induced micellization kinetics of diblock and triblock copolymers. In all cases the obtained dynamic traces were well-fitted with a double-exponential function, with the fast time ascribed to the formation of quasi-equilibrium micelles, and the slow time associated with relaxation into the final equilibrium micelles. For the triblock copolymer system it was found that the slow process proceeds mainly via unimer exchange mechanism as the corresponding relaxation time was concentration independent.[7] On the other hand, at elevated salt concentration the slow process of triblock copolymer micelle relaxation proceeds via micelle fusion/fission.[9] In most cases for diblock copolymer micelles, the slow relaxation time is found to be strongly concentration dependent. The process proceeds via micelle fusion/fission

*Corresponding author. E-mail: eed@case.edu.

Published on Web 03/18/2010

with an estimated activation energy decreasing with an increase of hydrophobic chain length. For a shorter hydrophobic block unimer exchange becomes active and dominates the slow relaxation process, with the relaxation time independent of polymer concentration. In another series, a nonsolvent-induced micellization of pyrene end-labeled diblock copolymers was studied via a combination of stopped-flow light scattering and fluorescence techniques.[11] The dynamic traces of scattered intensity were successfully fitted by double exponential functions with both fast and slow relaxation times decreasing with concentration. This indicates that both the formation of quasi-equilibrium micelles and the slow relaxation into final equilibrium micelles proceed primarily via the micelle fusion/fission mechanism. The excimer to monomer fluorescence emission intensity traces fitting required a triple exponential function with the two longer relaxation times being the same (and presumably reflecting the same processes) as obtained in the light scattering fit. The fast relaxation process, which could only be detected by the fluorescent technique contributed about 75% of initial emission intensity increase and was attributed to the fusion of small aggregates at the early stage of micellization. Fluorescence is very sensitive to small aggregates, while the corresponding scattering intensity change was very small due to small size of the aggregates at early times. Lund and co-workers[13] recently applied the high resolution synchrotron X-ray scattering technique to study the time-dependent aggregation number evolution following solvent jump. They also found that micellization proceeds quicker at higher polymer concentration and argue that there are multiple time scales associated with the micellization process.

Various theoretical models[14−19] have been developed to predict the diblock copolymer micelle growth mechanism in a selective solvent. Most of the models are based on free energy and potential barrier considerations. Some theoretical approaches[14,16,18,19] favor the unimer exchange mechanism, in which micelles grow mainly by the stepwise insertion of unimers into micelles because the potential barrier for polymer micelle fusion is considered to be too high compared to unimer exchange to play any role in micellization.[16,19] Since unimer exchange is limited by unimer expulsion, which is concentration independent, the corresponding relaxation time is concentration independent as well. According to the unimer exchange model, the aggregation number distribution should continuously evolve in a self-similar manner until equilibrium is reached. Semenov et al. pointed out that the micellization process driven by unimer exchange should be characterized by a continuous spectrum of relaxation times and the final equilibrium structures may never form.[19] Other theoretical models[15] favor the micelle fission/fusion mechanism, according to which micelles grow mainly by fragmentation and recombination of micelles. The micelle fusion probability increases and the corresponding relaxation time of the process decreases with an increase of polymer concentration as both the number of micelles increases and characteristic distance to travel before fusion decreases. One of us[17] proposed a joint analytical model for polymeric micelles that combines these two mechanisms. According to this model, the micellization process can be divided into three stages: during the first nucleation stage free unimers couple with each other very quickly; in the next stage fusion of micelles of comparable size becomes dominant while during the last stage micelles grow very slowly by both unimer exchange and fusion/fission of strongly nonequal size micelles. While these theoretical models shed light on the micellization process and provide background for experimental data interpretation, they often disagree on which kinetic mechanism is dominant under different conditions and how their predictions can be tested experimentally.

Computer modeling can provide the necessary background for testing analytical model predictions and can address both the large-scale macroscopic properties studied experimentally and molecular details discussed in analytical approaches. Ideally, both the micelle growth mechanism(s) and various kinetics-controlling factors of micellization can be studied if one can trace the movement of individual chains during the entire micellization process. Up to now, most simulation studies have focused on static properties of the micellar solutions, such as the critical micellar concentration (cmc), average micelle aggregation number, and the structure of micelles. There are only a few reports on the kinetics of micellization.[20−24] Mattice and co-workers[20] have used Monte Carlo simulations to study the evolution of dispersed unimers to form micelles. They investigated the evolution of number-average aggregation number and found that an increase of interaction energy or soluble block length results in freezing the self-assembly process at some metastable state.[20] By monitoring the change of unimer volume fraction, weight-average aggregation number and aggregation number of the large micelles, Wang and coauthors[21] found that the unimer volume fraction decreases very quickly to a stable level, while the weight-average aggregation number keeps slowly increasing before reaching a plateau level and may become frozen if there is a high degree of incompatibility between blocks. Pepin and co-workers[22] have analyzed autocorrelation times for chain extraction and exchange as a function of interaction energy for diblock copolymer micelles in the presence of a homopolymer solubilizate. Marrink and co-workers[23] applied atomistic molecular dynamics (MD) simulations to study formation of a single micelle from 54 dodecylphosphocholine (DPC) surfactant molecules in water. On the basis of three simulation runs, the dynamic processes of formation of a spherical micelle at low concentration of DPC molecules was investigated by monitoring the time evolution of the total number of aggregates, emergence and disappearance of aggregates of different size ranges during the spontaneous aggregation process. It was found that during the micellization process single surfactants frequently escape aggregates with a rate that is independent of cluster size. Chen et al.[24] recently applied a coarse-grained Brownian dynamics (BD) simulations with an implicit solvent model to study the self-assembly process of polystyrene-*b*-poly(ethylene oxide) copolymers into a single micelle in aqueous solution, aiming to compare the simulation results with flash nanoprecipitation experiments.[6] The evolution of the number of aggregates and the size of the largest aggregate in the course of unimer-to-micelle conversion has been monitored as a function of the friction coefficient. The overall micellization time was found to be considerably smaller than observed in experiments. The cluster size distribution and the average cluster size were investigated as a function of polymer concentration and cooling rate (which imitated the experimental rate of change of solvent quality).

In this paper, we study the kinetics of micelle formation from a randomly dispersed diblock copolymer solution using dissipative particle dynamics (DPD), a simulation method that combines MD and BD approaches.[25] DPD allows simulations on mesoscopic space and time scales, significantly exceeding the limits of molecular dynamic simulations while accurately addressing hydrodynamic interactions.[26,27] DPD has been successfully applied to reproduce and predict the phase behavior and properties of diblock copolymer melts and solutions, surfactant aggregates as well as complex self-assembled structures such as multicomponent micelles and polymersomes.[28−31] It has been demonstrated that DPD simulation can reproduce the scaling relationship for relaxation time and diffusion coefficients of polymers in both the melt and solutions with a chain length as short as 5,[27,32,33] making it possible to model the entire process of micellization with an explicit solvent. Sheng et al.[34] have recently applied DPD simulations to study the equilibrium properties of diblock copolymer micelles in dilute solution. They reported a polydisperse

micelle size distribution and investigated the micelle shape change and the scaling dependence of the average aggregation number and micelle radius on the soluble block length and the interaction parameters between the blocks and between insoluble block and solvent.

This paper is organized as follows. In the next section, we describe the details of our simulation approach. In the following section, we will discuss the equilibrium properties of the obtained micelles, such as cmc, aggregation number distribution, the average aggregation number and micelle structure as functions of oligomer concentration, interaction energy and hydrophilic block length. Then we will describe the general features and stages of the micellization process as well as discuss the contribution of different kinetic mechanisms of micelle formation. In the following section we will analyze the effects of different factors (oligomer concentration, interaction energy and block length) on the micellization kinetics. We will summarize our findings in the Conclusions.

Model and Simulation Details

To study the kinetics of micelle formation, we performed DPD simulations of short diblock copolymers (oligomers) self-assembling into spherical micelles in dilute solution. An oligomer was represented as a coarse-grained linear bead−spring chain A_mB_x with m hydrophobic (A) beads and x hydrophilic (B) beads. Solvent molecules were modeled as single beads identical to the hydrophilic block bead (B) in a model chain. All beads in our simulations had the same mass m_0 and diameter d_p which will be used as units of mass and length. All simulations were performed under periodic boundary conditions in a cubic box ($30d_p \times 30d_p \times 30d_p$) containing 81000 beads. This rather large box size was selected to accommodate a larger number of oligomers (and hence micelles at equilibrium) and to minimize the possible influence of box-size effects on polymer chain diffusion coefficient.[27] All monomers in a A_mB_x oligomer were linked by a harmonic bond force $\mathbf{f}_{bond} = k(r_{ij} - b_0)\mathbf{r}_{ij}/r_{ij}$, where the force constant[27,32,33] is $k = 100\ k_bT/d_p^2$, k_bT is unit of energy (k_b is the Boltzmann constant, T is temperature), r_{ij} and $\mathbf{r}_{ij}$ is the distance and vector between particle i and j, correspondingly and the equilibrium bond length is $b_0 = d_p$. The pairwise interaction forces between different beads included a conservative force, $\mathbf{f}^C$, dissipative force, $\mathbf{f}^D$, and random force, $\mathbf{f}^R$:

$$\begin{aligned}\mathbf{f}_{ij} &= \mathbf{f}_{ij}^{C} + \mathbf{f}_{ij}^{D} + \mathbf{f}_{ij}^{R} \\ &= [-a_{ij}(r_c - r_{ij}) - \gamma w^D(\mathbf{r}_{ij}/r_{ij}\mathbf{v}_{ij}) + \sigma w^R(\zeta_{ij}(\Delta t)^{-1/2})]\mathbf{r}_{ij}/r_{ij} \\ &\qquad \text{for } r_{ij} < r_c \end{aligned} \quad (1)$$

Here a_{ij} is the repulsion parameter, $\mathbf{r}_{ij}$ and $\mathbf{v}_{ij}$ are the distance and velocity vectors of the particle i with regards to particle j, $r_c = d_p$ is the cutoff distance for the conservative force, $\gamma = 3.0k_bT/d_p^2$ is the friction coefficient,[26] $\sigma = (2\gamma k_bT)^{1/2}$ is the noise amplitude, w^D and w^R are the weight functions ($w^D = (w^R)^2 = (r_c - r_{ij})^2$), ζ_{ij} is the Gaussian random number, and Δt is the time step. The density of all beads including polymer monomers and solvent was equal to $3d_p^{-3}$ and the repulsive interaction parameters between same type of beads were $a_{AA} = a_{BB} = 25k_bT/d_p^2$ to reproduce the compressibility of water at room temperature.[26] In the following, k_bT/d_p^2 will be omitted when referring to values of the interaction parameter a_{ij}. On the basis of the a_{BB} interaction parameter, the B-block is in a good solvent with the Flory exponent 0.6 observed for the homopolymer radius of gyration and diffusion coefficient.[27,33] The repulsive interaction parameter between different types of beads a_{AB} was larger than 25 to reflect the A−B hydrophobic interactions. Selection of absolute values of a_{AB} was made based on simulation test runs for different chains, A_2B_3 and A_4B_x ($x = 4, 6, 8$), to obtain spherical micelles, which are not kinetically frozen (i.e., chain exchange between micelles could be observed within the simulation time scale). For solutions of A_2B_3 chains, we varied the repulsive parameter ($a_{AB} = 47.5, 50, 52.5, 55$) and volume fraction of chains, φ, from 9.3×10^{-4} to 0.05 to study the kinetics of micelle formation. For solutions of A_4B_x chains, we kept the hydrophobic block length ($N_A = 4$) and the volume fraction of chains ($\varphi = 0.05$) constant, and varied the hydrophilic block length ($N_B = 4, 6, 8$) and repulsive parameter ($a_{AB} = 38, 40$) to study the chain length and hydrophobic interaction energy effects on the kinetics of micellization. Taking into account the relatively short chain lengths and low polymer concentrations considered, we will be exploring in this paper chain and micelle diffusion in solution (corresponding to Zimm regime) and core-block diffusion in the micelle core (corresponding to Rouse regime), both of which are well-reproduced using DPD.[27,32,33] In all simulations the NVT ensemble was adopted ($k_BT = 1$) and the equations of motion were integrated with a modified version of the velocity-Verlet algorithm[35] with time step $\Delta t = 0.04$ time units of $(m_0d_p^2/k_bT)^{1/2}$, which is omitted below.[26] We used a free-source code LAMMPS[36] for the DPD simulations on the HPC computer cluster at Case Western Reserve University.

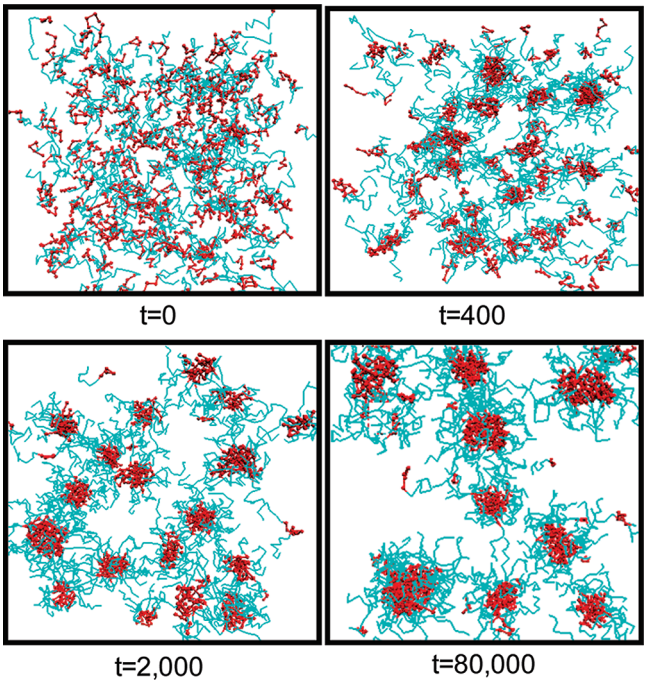

Figure 1. Snapshots of the simulation box containing A_4B_8 chains ($a_{AB} = 40$, $\varphi = 0.05$) obtained in the course of micelle formation (the hydrophobic block is shown by connected balls, the hydrophilic block is shown by connected bonds (i.e., balls omitted), solvent beads are not shown, rendered by VMD).

All DPD simulations started from a random dispersion of model chains in the solution. Initially we applied the repulsive parameter $a = 25$ for all pair interactions between the beads and after $t = 4 \times 10^4$ all the chains were homogeneously dispersed in the solution (Figure 1). Then the hydrophobic interaction was imposed by increasing a_{AB} to the desired value and the process of micelle formation was monitored. The movement trajectories were collected every 100 time steps for data analysis. We used VMD[37] for displaying movement trajectories and data analysis. In all simulation runs, we observed that the originally randomly dispersed free chains self-assemble into small aggregates very quickly, and then large spherical micelles gradually form during the course of simulations, as shown in Figure 1. To distinguish

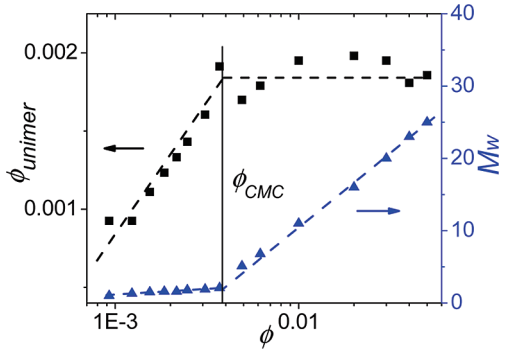

Figure 2. Weight-average aggregation number and unimer volume fraction as a function of oligomer volume fraction in A_2B_3 micellar solution (a_{AB} = 47.5) (Lines are guides for the eye only). The vertical line corresponds to the cmc at $\varphi \approx 3.7 \times 10^{-3}$.

different aggregates, we used a general distance criterion.[23] With this criterion, any pair of chains within a certain cutoff distance between the centers of mass of hydrophobic blocks belongs to the same aggregate. After testing the criterion on different systems, we determined that the result does not depend on the precise choice of the cutoff distance, and a general cutoff distance of $1.5d_p$ was used to distinguish different aggregates for all systems with A_2B_3 chains, and cutoff distance of $1.8d_p$ was used for aggregates composed of A_4B_x chains. In this way, the instantaneous affiliation of each chain, as well as the aggregation number and composition of each aggregate, are clearly determined. With all the aggregates identified, the number- (M_n) and weight-average (M_w) aggregation number of micelles was calculated as

$$M_n = \sum_i n_i P_i / \sum_i n_i, \quad M_w = \sum_i n_i P_i^2 / \sum_i n_i P_i \qquad (2)$$

where n_i is the number of aggregates (including unimers) containing P_i oligomers. By monitoring the time-dependent weight-average aggregation number, the equilibrium state of the micelle solution was determined (when the average aggregation number reaches a plateau level with deviations less than 15% of the average value). The simulations were conducted for an additional period of time to characterize the equilibrium properties of the micellar solution. For solutions with A_2B_3 chains, the simulation time for each system at equilibrium was about $t = 3.2 \times 10^5$, and for systems with A_4B_x chains, it was about $t = 1.2 \times 10^6$. In the polymer volume fraction range studied ($\varphi \leq 0.05$), all final micelles had spherical form.

Simulation Results and Discussion

We first characterize the equilibrium properties of the obtained micellar solution, including the critical micelle concentration, micelle aggregation number distribution, and micelle structure, for different oligomer number densities, hydrophobic interaction energies, and chain lengths.

Equilibrium Properties

Critical Micellar Concentration. In a selective solvent diblock copolymer molecules aggregate spontaneously into micelles when the concentration is above the critical micelle concentration (cmc). As micelle formation does not represent a phase transition, the definition of cmc is somewhat arbitrary and may depend on the criteria applied.[3,21,24,38−42] To determine the cmc for A_2B_3 micellar solution with repulsive parameter a_{AB} = 47.5, we calculated the weight-average aggregation number and the volume fraction of unimers and small aggregates in a range of system compositions $\varphi = 9 \times 10^{-5}$ to 0.05. The fraction of unimers (and other small aggregates) increases with oligomer volume fraction and reaches a plateau level at about $\varphi \approx 3.7 \times 10^{-3}$, as is seen in Figure 2. At that point, the weight-average aggregation number starts to rapidly increase. Thus, based on the behavior of both the unimer volume fraction[21,40,42] and weight-average aggregation number, we determined that cmc for this case is $\varphi \approx 3.7 \times 10^{-3}$. We note that the plateau level for unimer volume fraction (about 1.9×10^{-3}) is lower than the cmc value because of the contribution of small aggregates such as dimers, trimers, etc.[42] Such small aggregates exist (in addition to unimers) over the whole concentration range considered and their volume fraction reaches plateau levels at different oligomer concentrations (see Supporting Information). Thus, the cmc represents an equilibrium between unimers, small aggregates and larger micelles and can be identified by the appearance of large micelles in the aggregation number distribution, as proposed by Ruckenstein et al.[38] Indeed, comparing the aggregation number distribution at oligomer volume fractions below and above the cmc ($\varphi \approx 3.7 \times 10^{-3}$) we observe above the cmc the appearance of a shoulder and/or a peak at higher aggregation numbers, whereas below the cmc the distribution shows an exponential decay behavior (see Supporting Information). It is worthwhile to note that the cmc depends on the hydrophobic interaction energy parameter and chain length: as a_{AB} increases or corona block length decreases (which leads to an increase of the average aggregation number), the cmc decreases.[21,41−43] For comparison, we listed the unimer concentration at equilibrium for different micellar systems considered in this paper (at φ = 0.05) in Table 1.

Table 1. Equilibrium Aggregation Number Determined from Number- and Weight-Average Aggregation Number Distributions $M_{n,peak}$ and $M_{w,peak}$, Number- and Weight-Average Aggregation Number $M_n$and M_w (Eq 2), and Unimer Volume Fraction φ_{unimer}, for A_2B_3 Micellar Solutions with Different Interaction Parameters a_{AB} and for A_4B_4, A_4B_6, and A_4B_8 Micellar Solutions for $a_{AB} = 40$ (φ = 0.05 in All Cases)

oligomer	a_{AB}	$M_{n,peak}$	$M_{w,peak}$	M_n	M_w	φ_{unimer} $(\times 10^4)^a$
A_2B_3	47.5	24 ± 7	26 ± 6	10 ± 1	25 ± 2	19.0 ± 0.6
A_2B_3	50	31 ± 6	33 ± 6	16 ± 1	32 ± 1	9.9 ± 0.5
A_2B_3	52.5	36 ± 6	37 ± 5	24 ± 3	38 ± 2	4.9 ± 0.1
A_2B_3	55	43 ± 8	43 ± 5	32 ± 3	41 ± 2	2.8 ± 0.4
A_4B_4	40	51 ± 6	55 ± 7	32 ± 5	54 ± 4	4.9 ± 2.9
A_4B_6	40	38 ± 4	40 ± 4	21 ± 3	38 ± 3	8.9 ± 3.3
A_4B_8	40	31 ± 4	34 ± 3	15 ± 2	31 ± 2	12.9 ± 4.3

[a] For all A_2B_3 micelle solutions φ_{unimer} was calculated for a given a_{AB} by averaging over different volume fractions, while for A_4B_x micelle solutions it was calculated by averaging over time.

Micelle Aggregation Number Distribution. The number- and weight-average aggregation number distributions were calculated based on the occurrence probability of aggregates collected over the entire time range of equilibrium micelle state simulations. Figure 3 shows the weight-average aggregation number distribution for A_2B_3 micellar solutions for different interaction energies and for A_4B_x micelle solutions for different B-block lengths (a_{AB} = 40) at oligomer volume fraction φ = 0.05. As is seen, all distributions are relatively smooth and exhibit one minimum and one maximum, indicating equilibrium between unimers (and small aggregates) and larger micelles. The maximum of the distribution corresponds to the thermodynamically preferable micelle aggregation number under the specific conditions. For A_2B_3 micellar solutions at different oligomer volume fractions, the preferable aggregation numbers and the corresponding

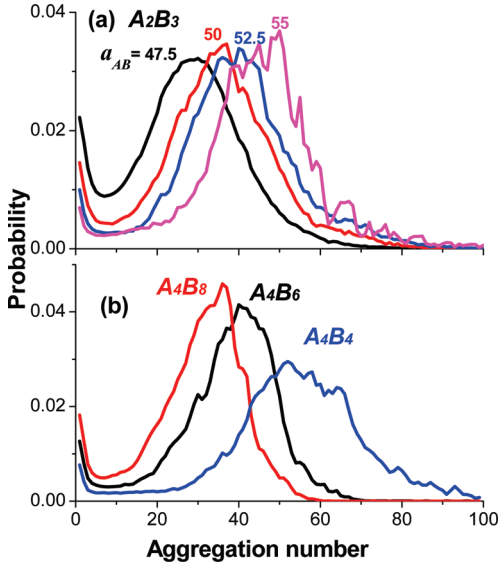

Figure 3. Weight-average aggregation number distribution for (a) A_2B_3 micellar solutions with different interaction energies a_{AB} = 47.5, 50, 52.5, 55 and (b) for A_4B_4, A_4B_6, and A_4B_8 micellar solutions (a_{AB} = 40) for oligomer volume fraction φ = 0.05.

distribution peaks are nearly the same.[39,42] For lower oligomer volume fractions the probability of finding small aggregates is slightly higher and the corresponding average aggregation number is slightly lower (see Supporting Information) as expected for micellar solutions well above the cmc.[3] With an increase in the interaction energy a_{AB} the equilibrium aggregation number for A_2B_3 micelles increases and the peak position of the distribution shifts to higher values (Figure 3a). An increase in a_{AB} (which is related to the interfacial tension[3]) implies the larger incompatibility with a solvent (and corona block) that drives the chain self-assembly to form larger micelles in order to minimize the interfacial tension. The aggregation numbers at peak positions $M_{w,peak}$ and $M_{n,peak}$ of the weight- and number-average aggregation number distributions were calculated by fitting the peak area with normal distribution. Table 1 shows the results for A_2B_3 micellar solutions at the same oligomer volume fraction (φ = 0.05) for different interaction energies (a_{AB} = 47.5, 50, 52.5, 55). As is seen, the values of $M_{n,peak}$ and $M_{w,peak}$ are rather similar for a given a_{AB} value. For comparison, the corresponding number-average M_n and weight-average aggregation numbers M_w (see eq 2) are also listed in the Table 1. Since M_n includes all the aggregates and unimers, it is lower than $M_{n,peak}$ calculated by fitting the high-end of the aggregation number distribution. With an increase in a_{AB} the minimum of the distribution becomes broader and the probability of finding unimers or small aggregates decreases (Figure 3a). The corresponding volume fractions of unimers for the micellar solutions are listed in Table 1. As is seen, increasing the hydrophobic interaction energy causes the average aggregation number to increase and average unimer concentration to decrease. Similar results have been observed in DPD and Monte Carlo simulations of diblock copolymer micelle solutions.[34,40−42]

To investigate the effect of hydrophilic block length we have varied the B-block lengths, N_B = 4, 6, and 8, while keeping core block the same, N_A = 4. The weight-average aggregation number distributions for A_4B_4, A_4B_6 and A_4B_8 micellar solutions (φ = 0.05, a_{AB} = 40) are shown in Figure 3b. As is seen, the longer the hydrophilic block length, the smaller the equilibrium aggregation number[43] and the more narrow the distribution. The observed decrease in the aggregation number is due to the larger loss in conformational and translational entropy for a longer chain to become part of a large micelle. Qualitatively similar results were observed experimentally[12,44] and in computer simulations of block copolymer micelles.[34,42] The decrease in the average aggregation number with an increase in B-block length shown in Figure 3b is accompanied by the increase in the fraction of unimers and small aggregates. Table 1 lists the equilibrium aggregation numbers, weight- and number-average aggregation numbers and unimer volume fraction.

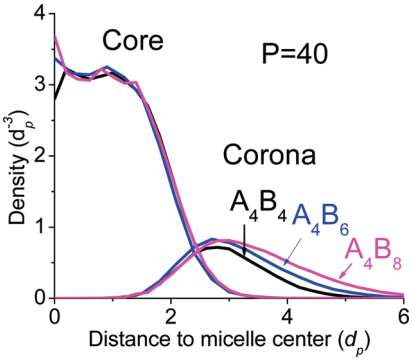

Figure 4. Monomer density profiles for core and corona of A_4B_4, A_4B_6, A_4B_8 micelles of aggregation number P = 40 (φ = 0.05, a_{AB} = 40).

Micelle Structure. To characterize the structure of the micelles obtained in our simulations, the density profiles of the micelle core (hydrophobic blocks) and corona (hydrophilic blocks) were calculated as a function of the distance from the micelle center of mass. Figure 4 shows the density profiles for A_4B_4, A_4B_6, and A_4B_8 micelles with the same aggregation number P = 40, (a_{AB} = 40, φ = 0.05). The density profiles for the core monomers are practically the same for all three cases. The plateau value of the hydrophobic beads density inside the core is close to 3, implying that there are no hydrophilic beads or solvent inside the core (one can recall that the density in our simulations was equal to $3d_p^{-3}$). The core/corona interfaces are very similar in all cases with interfacial width being about d_p (i.e., comparable to the bond length). The main difference seen in the density profiles concerns the monomer density in the corona: as the hydrophilic block length increases, the monomer density in the corona extends to a larger distance. The density profiles of A_2B_3 micelles of the same aggregation number with different interaction energies a_{AB} do not show obvious difference (see Supporting Information). Similar monomer density profiles were obtained in Monte Carlo simulations of diblock copolymer micelles.[2,21,40−42] All micelles observed in our simulations were of a spherical shape except for the transient (nonstable) aggregates formed just after micelle fusion or just before micelle fission.

Micellization Kinetics

We will first discuss using the example of a A_2B_3 solution the general features and possible mechanisms of the micelle formation process from unimers and then investigate the influence of different factors such as oligomer concentration, interaction energy and block length, on the kinetics of the micellization process.

Molecular Mechanism of Micellization. As discussed in Model and Simulation Details, we studied the process of oligomer self-assembly into spherical micelles starting from a homogeneously dispersed unimer solution. This was accomplished by increasing the interaction energy a_{AB} from 25

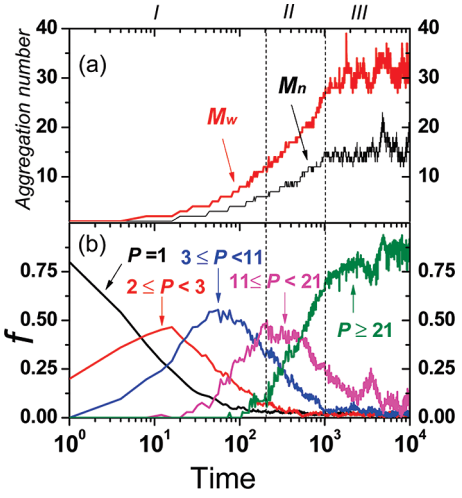

Figure 5. (a) Number- and weight-average aggregation numbers and (b) weight-average fraction of aggregates in different size ranges as a function of time during the process of micelle formation in A_2B_3 solution (a_{AB} = 50, φ = 0.05). Vertical dashed lines indicate the approximate boundaries between different stages of micellization process.

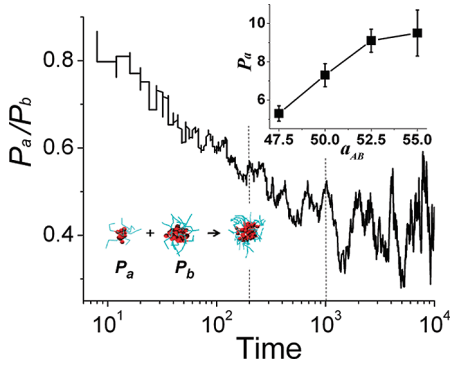

Figure 6. Ratio of aggregation numbers of small to large reactants in the micellization addition process of A_2B_3 (a_{AB} = 50, φ = 0.05, corresponding to Figure 5) as a function of time. Vertical dashed lines indicate the approximate boundaries between different stages of the micellization process. The inset shows the average aggregation number of the smaller reactant during the final stage of micellization as a function of a_{AB}.

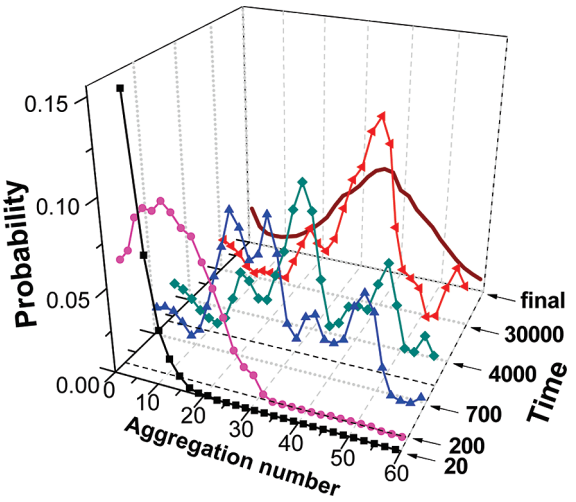

Figure 7. Weight fraction aggregation number distribution during the micellization process of A_2B_3 solution (a_{AB} = 50, φ = 0.05, corresponding to Figure 5). Curves with symbols for different time steps are the running average. The equilibrium distribution is shown as a curve without symbols. Horizontal dashed lines indicate the approximate boundaries between different stages of micellization process.

(neutral solvent/B-block interactions) to larger values (bad solvent for A, repulsive interactions with B-block) at t = 0. The progress of unimer self-assembly into micelles can be characterized by monitoring the average micelle aggregation number as a function of time, similar to what has been done experimentally,[4,13] starting from the very early stages of micellization. Figure 5a shows both the number- and weight-average aggregation numbers as functions of time during the micellization process for A_2B_3 solution with a_{AB} = 50 at the oligomer volume fraction φ = 0.05 for a typical simulation run.

As is seen M_n and M_w quickly increase until reaching their respective equilibrium plateau level.[20,21,23,24,34] As will be discussed below, equilibration of the number-average aggregation number occurs quicker than M_w. Besides the macroscopic characteristics of the process we can also obtain from our simulations the time-dependent population of different aggregates.[17,23] Figure 5b shows the time evolution of the weight fraction of different aggregates, which for clarity were grouped into size ranges. As is seen, early in the micellization process the fraction of unimers decreases very quickly as they merge into small aggregates and the average aggregation number starts to increase. As time goes by, larger aggregates start to appear while the fraction of small aggregates declines. At this stage redistribution of chains occurs very actively and the average aggregation number continues to increase. At the later stages of micellization most of the chains exist in large micelles and the number- and weight-average aggregation numbers stabilize, dominated mainly by the contribution of large micelles.

In order to distinguish the contributions of different mechanisms of micellization over the course of time, we subdivide the micellization into three stages similar to our earlier analytical model.[17] During the first stage the unimer concentration decreases very sharply and stabilizes at about $t \approx 100 - 200$ (Figure 5b). During this stage unimers couple with each other forming dimers, which can also merge with each other or unimers. Figure 6 shows the time-dependent aggregation number ratio between the smaller reactant (with aggregation number P_a) and the large reactant (with aggregation number P_b) in all aggregate addition reactions. An aggregate addition reaction is defined as the process of merging of two reactants (including unimers) a and b with aggregation numbers P_a and P_b with the formation of a new aggregate, which lasts for at least two statistical time intervals ($=200\Delta t$). The smaller aggregate (which can be a unimer) in the reaction is labeled as "a" and the larger one as "b". If we have reaction between reactants of the same size then the ratio P_a/P_b will be 1. Thus, the smaller is the ratio the larger is the disparity in the sizes of aggregates participating the reaction.

As is seen, during the first stage of micellization the reactant ratio decreases from about 0.9, indicating mainly the merger of equal aggregates, to about 0.55, where fusion of aggregates of nonequal sizes starts to play a role. These findings agree well with the scenario of micellization predicted in an earlier analytical model by one of us[17] and with the results of a recent experimental study on solvent-jump micellization of a pyrene end-labeled diblock copolymers.[11] In the latter study, it was found that the fastest relaxation process, which contributed about 75% of the initial emission intensity increase, is attributed to the fusion of small aggregates at the early stage of micellization.[11] As is seen from Figure 5, during the first stage of micellization only rather

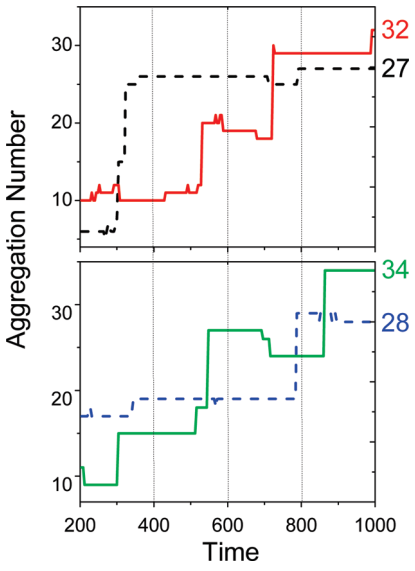

Figure 8. Time evolution of the aggregation number P of selected individual micelles during the second stage of micellization process of A_2B_3 solution ($a_{AB} = 50$, $\varphi = 0.05$).

small aggregates are formed with the weight-average aggregation number being about 10 by the end of this stage after most unimers are consumed.

At the beginning of the second stage of micellization the average aggregation number is far from the equilibrium value and the weight-average aggregation number distribution exhibits just a single maximum around the average aggregation number (of about 10), as is seen in Figure 7. As time goes by, the fraction of small aggregates decreases and large micelles start to form and become dominant. The ratio of aggregation numbers between the reactants in the aggregate addition reaction continues to decrease (Figure 6). Micelle fusion between aggregates of nonequal sizes and the increasing contribution of unimer exchange are the main contributing factors. By the end of the second stage of micellization, the number-average aggregation number reaches its equilibrium level (Figure 5), indicating that the total number of aggregates has equilibrated, while the weight-average aggregation number continues to increase. The ratio of aggregation numbers between reactants in the aggregate addition reaction also reaches a plateau value (about 0.4) by the end of the second stage (Figure 6) indicating that the process of active micelle growth is finalized. It is interesting to note that by the end of the second stage the weight fraction aggregation number distribution exhibits two maxima, one below (P $\approx$ 27) and one above (P $\approx$ 50) the equilibrium aggregation number, $P_{eq} \approx 33$, (Figure 7).

To investigate the growth pathways during the second stage of micellization we trace all the micelles with the characteristic aggregation number ($25 < P < 35$) at t = 1,000 back to the earlier times. The predecessor of a micelle was defined as the micelle which contains more than half the chains on the previous time step. The statistical interval was chosen to be $100\Delta t$ to ensure correct counting of the instantaneous change of the micelles. In Figure 8, the time evolution of the aggregation number of some representative micelles is shown during the second stage of micellization. As is seen for all micelles, the aggregation number increases mainly by a few fusion events, normally 3−4, between micelles of comparable sizes, so that the instantaneous aggregation number exhibit large jumps. Further refinement of the aggregation number occurs via fission events involving

Table 2. Relative number of events (frequency) and fraction of chains exchanged (contribution) in the events involving unimers, small aggregates and micelles for stages II and III of the micellization process of A_2B_3 micellar solution ($\varphi = 0.05$, $a_{AB} = 50$), averaged over several simulation runs

	stage II		stage III	
process involving	frequency (%)	contribution (%)	frequency (%)	contribution (%)
unimers	61 ± 4	24 ± 6	69 ± 1	31 ± 2
small aggregates ($2 \le P \le 4$)	21 ± 6	22 ± 7	22 ± 1	25 ± 2
micelles ($P \ge 5$)	18 ± 10	54 ± 12	9 ± 1	44 ± 4

expulsion of a small aggregate or by unimer expulsion. The bimodal weight-average aggregation number distribution shown in Figure 7 is the result of such an active micelle fusion process. If the micelle formation process involved unimer insertion only then one would expect a smooth evolution of the distribution to the final one without a significant change of its shape or especially formation of micelles of larger than equilibrium size.

A qualitatively similar micelle size evolution as shown in Figures 7 and 8 was also observed for longer chains (A_4B_x), as will be discussed below (see also Supporting Information). These results demonstrate the importance of the contribution of micelle fusion to the process of micelle formation and are in accord with recent experimental observations.[6,10,11] In rapid micromixing homogeneous precipitation experiments, Johnson and co-workers[6] found that under the conditions of a slow solvent quality change both unimer exchange and micelle fusion take place during the micellization process. The analysis of dynamic traces of light scattering intensity obtained by Liu and co-workers in their study of diblock copolymer micellization kinetics induced by pH-jump[10] and solvent-jump[11] revealed that in many cases both the fast and slow relaxation times decrease with concentration, indicating that both the formation of quasi-equilibrium micelles and the slow relaxation into final equilibrium micelles proceed primarily via micelle fusion/fission mechanism.

We have also analyzed our data to characterize the frequency of occurrence of different processes, such as unimer exchange or micelle fusion/fission, during the second stage of micellization. Strictly speaking unimer exchange involves single chain insertion/expulsion or exchange between micelles and for the second stage of A_2B_3 micellization in solution ($\varphi = 0.05$, $a_{AB} = 50$) its probability of occurrence was about 60%, as is seen from Table 2 while the rest (40%) can be attributed to collective micelle fusion/fission events. Thus, both processes make a considerable contribution to micellization. At the same time if one considers the number of chains exchanged by either of the processes, then unimer exchange was responsible for only 24% with the majority (76%) of chains being exchanged by collective micelle fusion/fission. Hence we can conclude that contribution of micelle fusion/fission was dominant in this stage of micellization, in agreement with recent experimental findings.[10,11]

As discussed above, the cmc reflects not only unimers but also small aggregates. We have separated the contribution of small aggregates ($2 \le P \le 4$) into the micellization process in Table 2. We note that the choice of the upper size boundary for small aggregates was dictated by the position of the minimum in micelle size distribution (Figure 3). As is seen from Table 2 expulsion/insertion and exchange of small aggregates between micelles contributed about 20% of events and 20% of exchanged chains. It is worthwhile to note that if one considers "unimer exchange" more broadly and includes processes involving small aggregates, then it

becomes the dominant process regarding the probability of occurrence, but it contributes less than 50% to chain exchange. Processes involving small aggregates play an important role in the micellization kinetics as will be discussed below. The small aggregate contribution to micelle formation process has recently been detected for pyrene end-labeled diblock copolymers studied via a combination of stopped-flow light scattering and fluorescence techniques.[11] Because of the high sensitivity of the fluorescent technique to small aggregates a third relaxation time attributed to the fusion of small aggregates has been determined (in addition to the two slower relaxation times obtained from light scattering) and is found to be concentration dependent.

At the beginning of the third stage ($t \approx 1000$), the aggregation number distribution reflects a bimodal population of micelles (Figure 7) with aggregation numbers somewhat larger ($P \approx 50$) or smaller ($P \approx 27$) than the final equilibrium number ($P \approx 33$). At this time the number-average aggregation number is practically equilibrated, implying that the number of aggregates has reached the thermodynamically preferred value, while the weight-average aggregation number is somewhat smaller than the equilibrium value. Thus, the main development of the last stage of micellization process is redistribution of chains among micelles to achieve the equilibrium weight-average aggregation number distribution. As is seen from Figure 6 the ratio of aggregation numbers of reactants in aggregate addition reactions does not appreciably change (compared to the previous stages of micellization), but fluctuates strongly indicating participation of different size reactants in the process. Statistical analysis of different events occurring during the last stage of micellization shows that unimer exchange becomes more dominant, with its probability of occurrence increasing to about 70%. Exchange of small aggregates ($2 \leq P \leq 4$) between micelles remains at a comparable level (about 20%) and the probability of micelle fusion declines (9%). The latter is not surprising as the number of micelles is considerably smaller and their size is bigger. Still, the contribution of micelle fusion into overall chain redistribution remains at considerable level − 44% of chains are exchanged via micelle fusion, which is larger than either the contribution of unimer exchange (31%) or processes involving small aggregates (25%). This is in agreement with experimental findings by Johnson and co-workers[6] and Liu and co-workers who studied the diblock (and triblock) copolymer micellization kinetics induced by pH-jump[7,9,10] and solvent-jump:[11] in most of the cases the slow relaxation time was found to be strongly concentration dependent, indicating that micelle fusion/fission plays an important role in the slow relaxation into the final equilibrium micelles. The weight-average aggregation number distribution, which still exhibits a bimodal shape at the earlier times of the final stage of micellization, gradually becomes unimodal with the peak position corresponding to the final equilibrium aggregation number (Figure 7). The analysis of time evolution for individual micelles (similar to Figure 8) shows that fusion of large micelles becomes rather rare (but still can be seen even at equilibrium) and normally involves a fission event immediately afterward. In general the dynamic features of the last stage of micellization are rather similar to the equilibrium chain-exchange dynamics of a micellar solution.

It is important to note that micellization is a continuous process, and our purpose in designating stages is merely to distinguish the most representative pathways of micelle growth. During the first two stages, which proceed noticeably quicker compared to the last stage, the major part

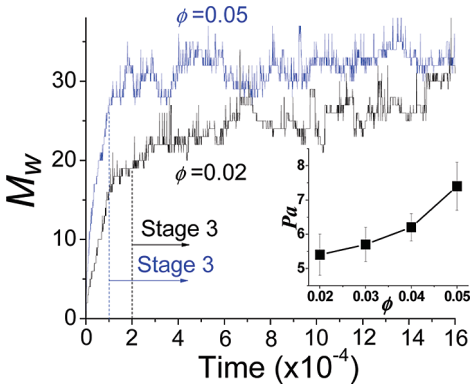

Figure 9. Time evolution of the weight-average aggregation number during the micellization process of A_2B_3 solution ($a_{AB} = 50$) for different oligomer volume fractions $\varphi = 0.02, 0.05$. Vertical shaded lines indicate the beginning of the third stage of micellization for each curve. The inset shows the average aggregation number of the smaller reactant in addition reactions (similar to Figure 6) during the final stage of micellization as a function of φ.

(about 75%) of micelle growth is accomplished by fusion of small unstable aggregates. The probability of aggregate encounter is high and the energy barrier for fusion is low, such that the contribution of micelle fusion is considerable at this stage. As the micellization progresses to the last stage, the average size of micelles increases and their number decreases to nearly the equilibrium value, making it less likely for large micelle fusion to occur. Still, micelle fusion/fission together with unimer and small aggregate exchange all contribute to the slow process of weight-average aggregation number growth/adjustment. The boundaries between different stages and the relative contribution of different kinetic processes to micellization depend on the system properties, such as block ratio, interaction between blocks and solvent, polymer concentration, block length, etc. The influence of some of these parameters on micellization kinetics will be discussed below.

Concentration Effect. The time-evolution of the weight-average aggregation number during the micellization processes of A_2B_3 solutions (with interaction energy $a_{AB} = 50$) is shown in Figure 9 for different oligomer volume fractions: $\varphi = 0.02, 0.05$. As is seen, the growth of the weight-average aggregation number occurs in a qualitatively similar way: a rapid increase in the beginning and gradual saturation to a plateau level later on. Comparing the time-scales of different stages of the process at different oligomer volume fractions one can find that an increase in oligomer content speeds up the micellization process: e.g. it takes almost twice the time to reach stage 2 or stage 3 of the micellization at $\varphi = 0.02$ (end of the first stage $t \approx 400$, end of the second stage $t \approx 2000$) compared to $\varphi = 0.05$ (end of the first stage $t \approx 200$, end of the second stage $t \approx 1000$). Correspondingly equilibrium is reached noticeably quicker at higher oligomer content. This observation is consistent with the results of recent X-ray experiments[13] and analytical predictions.[18] One of the reasons for this effect is that the denser is the solution, the shorter the distance for chains and aggregates to travel before they can merge with each other. Also a larger number of aggregates increases the probability of micelle fusion, which is one of the important components of the micellization process. The frequency of micelle fusion/fission during the second stage of micellization increases by 50% and the fraction of chains exchanged via micelle fusion/fission mechanism during the third stage of micellization doubles upon an increase in oligomer

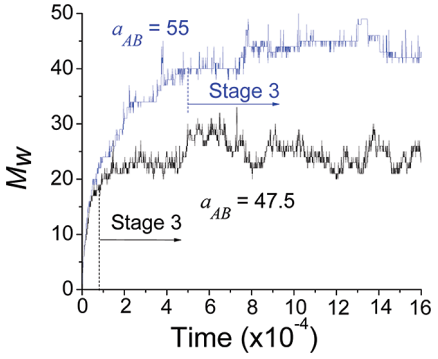

Figure 10. Time-evolution of the weight-average aggregation number in the course of micellization of A_2B_3 solution ($\varphi = 0.05$) for different interaction energies $a_{AB} = 47.5, 55$. Vertical shaded lines indicate the beginning of the third stage of micellization.

volume fraction from $\varphi = 0.02$ to $\varphi = 0.05$ (cf. Table 2 with Table S1 in the Supporting Information). The strong concentration dependence of the slowest relaxation time associated with micelle fusion/fission has been observed in a series of pH-jump[7,9,10] and solvent-jump[11] experiments as well as computer simulations.[45] Our simulations show that for a low oligomer concentration the weight-average aggregation number distribution exhibits primarily a single maximum (not shown) evolving toward the equilibrium value, which is consistent with a strong contribution of unimer (and small aggregate) exchange in this case. The size of the smaller reactant (which includes unimers) in addition reactions consistently increases with an increase in oligomer volume fraction, as is seen in Figure 9 (inset). Thus, an increase in oligomer content enhances probability of micelle fusion/fission events and speeds up the micellization process.

Hydrophobic Interaction Energy Effect. The time-evolution of the weight-average aggregation number during the course of micellization of A_2B_3 solutions ($\varphi = 0.05$) with different interaction energies ($a_{AB} = 47.5, 55$) is compared in Figure 10. At the very early times, the micelle growth occurs following nearly the same pathway independent of the interaction energy. The difference in the micellization process lies in the later times, when micellization of oligomers with higher interaction energies is noticeably slower ($a_{AB} = 47.5$: end of the first stage $t \approx 200$, end of the second stage $t \approx 800$, $a_{AB} = 55$: end of the first stage $t \approx 200$, end of the second stage $t \approx 5000$). We have also analyzed and compared the micellization process for A_4B_x systems with different interaction energies ($a_{AB} = 38$ and 40). In all cases the corresponding time windows for the first, second and third stages of micellization noticeably expand with an increase in a_{AB}. One reason for this effect is that the higher interaction energy implies higher equilibrium aggregation number (Figure 3 and Table 1), which requires a larger number of events (unimer exchange, micelle fusion/fission). Also the potential barrier for unimer expulsion or micelle fission is higher for larger a_{AB},[16,17,19] which would slow down the micellization process as well. Similar observations have been made in stop-flow experiments of nonsolvent-induced micellization[11] and in computer simulations[20] as well as been predicted analytically.[19] The analysis of the statistics of micelle evolution (performed for both A_2B_3 and A_4B_x systems) show that the frequency of occurrence and contribution of unimer exchange to the micellization process generally increase with an increase in a_{AB}, especially during the final stage of micellization. Correspondingly, the frequency and contribution of processes involving small aggregates decrease. The frequency and contribution of micelle fusion/fission remains practically unaffected by the increase in a_{AB}. On one hand the larger average micelle size achieved by the end of the second stage of micellization for larger a_{AB} can make fusion somewhat less likely to occur, but on the other hand it is more efficient i.e. more chains are exchanged per event, as is seen from Figure 6 (inset). The contribution of micelle fusion to the last stage of micellization also does not appreciably change with an increase in a_{AB} for A_4B_x systems.

Table 3. Relative Number of Events (Frequency) and Fraction of Chains Exchanged (Contribution) in the Events Involving Unimers, Small Aggregates and Micelles for Stages II and III of the Micellization Process of A_4B_6 Micellar Solution ($\varphi = 0.05$, $a_{AB} = 40$), Averaged over Several Simulation Runs

	stage II		stage III	
process involving	frequency (%)	contribution (%)	frequency (%)	contribution (%)
unimers	81 ± 2	52 ± 5	88 ± 2	68 ± 1
small aggregates ($2 \le P \le 4$)	14 ± 2	21 ± 2	10 ± 2	18 ± 4
micelles ($P \ge 5$)	5 ± 1	27 ± 4	2 ± 1	14 ± 5

Block Length Effect. Comparing the process of micelle self-assembly from unimers for A_4B_x and A_2B_3 solutions, one can conclude that the overall process proceeds via the same stages, as discussed above. In general the time window for the different stages expands with an increase of oligomer length, while the frequency and contribution of unimer exchanges increases and probability of micelle fusion/fission decreases (cf. Tables 2 and 3). The time evolution of the aggregation number of selected micelles shows fewer fusion/fission events, but otherwise is qualitatively similar to Figure 8 (see Supporting Information). We note that the oligomer volume fraction was $\varphi = 0.05$ for all A_4B_x systems, implying a smaller number of chains and micelles at equilibrium (for similar average aggregation numbers) compared to A_2B_3 micelle solution at the same polymer volume fraction. The decrease in the number of aggregates is a contributing factor to the overall micelle fusion/fission decrease. At the same time, the fraction of chains exchanged by micelle fusion/fission remains substantial (15−35%), as is seen from Table 3 and Table S2 in Supporting Information, so that this mechanism of micelle growth and chain exchange remains active. Comparing the aggregation number distribution at different time steps for A_4B_6 system we also observe a bimodal distribution at intermediate time steps similar to Figure 7 (see Supporting Information), which serves as an additional confirmation of importance of micelle fusion in the micelle growth process and the similarity of micelle formation for A_4B_x and A_2B_3 solutions. Another common feature of the micellization kinetics in all cases is a noticeable contribution of the processes involving small aggregates ($2 \le P \le 4$), which account for 20−30% of chains exchanged.

Comparing the micellization process for oligomers with the same hydrophobic block and different hydrophilic block lengths, one can expect that different kinetic processes may be affected to a different extent. For instance, one can imagine that micelle fusion may become less likely as a larger corona may prevent the core contact necessary for micelle merging. Statistical analysis of micelle evolution (for both $a_{AB} = 38$ and $a_{AB} = 40$) reveals that for systems with a longer hydrophilic block the overall number of kinetic events decreases, while the relative frequency of different events remains at comparable levels (cf. Table 3 and Table S2 in the Supporting Information). This is likely the outcome of several counteracting factors: e.g., oligomers with a longer hydrophilic block (which could negatively affect the

likelihood of micelle fusion) will form smaller micelles in equilibrium, as discussed above (which would make micelle fusion easier). There is a slight indication that with an increase in corona-block length the contribution of unimer exchange to the micellization process may even decrease while the fraction of chains exchanged via micelle fusion/fission may slightly increase. In general, the size of the smaller aggregates participating in aggregate addition reactions decreases with an increase of hydrophilic block length (see Supporting Information), while the ratio of reactants in aggregate addition reactions P_a/P_b increases. The first two stages of micellization process, i.e., consumption of unimers and equilibration of M_n often proceed slower for the system with longer hydrophilic block as a result of the lower diffusion coefficient (see Supporting Information) and larger distance to travel between unimers. At the same time the overall micellization process can often take a comparable time as oligomers with shorter hydrophilic block (such as A_4B_4) are prone to considerable fluctuations in aggregation number, which is larger at equilibrium (compared to A_4B_6 or A_4B_8 cases). It is important to emphasize that the fractions of chains exchanged via micelle fusion (15−35%) or processes involving small aggregates (~20%) in all cases add up to 32−60% (see Table 3 and Table S2 in the Supporting Information) indicating the importance of these processes in the kinetics of micelle formation.

Conclusions

Using the DPD simulation technique we studied both the equilibrium properties and kinetics of micelle formation from a randomly dispersed state to a well-equilibrated micellar solution. In agreement with previous reports, DPD simulation is found to be a very efficient simulation technique to study the equilibrium properties of diblock copolymer micelle solutions.[34] The cmc of the block copolymer solution was determined in our simulations by the shared transition point where the unimer concentration stabilizes and the average aggregation number increases sharply with an increase in φ due to the formation of large micelles. We found that the cmc exceeds the unimer concentration at equilibrium due to the contribution of small aggregates (dimers, trimers, etc.),[42] which were found to play a very important role in the overall dynamics of micelle solutions, as discussed below. We obtained the aggregation number distributions for micellar solutions of A_2B_3 and A_4B_x (x = 4, 6, 8) diblock copolymers. In all cases the aggregation number distribution was rather smooth and exhibited one minimum and one maximum, indicating equilibrium between unimers (and small aggregates) and larger micelles. We found, as is expected, that increasing the polymer concentration does not change the average aggregation number, while increasing the hydrophobic interaction energy or decreasing the hydrophilic block length causes the unimer concentration to decrease and the average aggregation number to increase.

The kinetics of the micellization process was analyzed by monitoring the time-evolution of the average aggregation number and fraction of aggregates of different sizes. We find that micellization can be characterized as a three-stage process (Figure 5). At the earliest stage, the unimer concentration decreases sharply to a constant value due to the rapid coupling of unimers into small aggregates. A close examination of the aggregation number evolution of individual micelles during the second stage (Figure 8) clearly indicates that micelles grow mainly by fusion of submicelles with intermediate aggregation numbers, in agreement with an earlier analytical model by one of us.[17] As a result of the active micelle fusion process the aggregation number distribution starts to exhibit a bimodal character with two maxima, above and below the equilibrium aggregation number (Figure 7). As micellization progresses the ratio of aggregation numbers between aggregates in addition reactions (including unimers) decreases (Figure 6) indicating that fusion of unequal size micelles or unimer exchange become more active. Analysis of the frequency of different events indicates that the processes involving small aggregates (dimers, trimers, etc.) play an important role in the micelle growth process. This finding agrees well with recent experimental data for pyrene end-labeled diblock copolymers studied via a combination of stopped-flow light scattering and fluorescence techniques.[11] Micelle fission/fusion is the most efficient mechanism of micelle growth during the second stage (e.g., the number of chains exchanged by this mechanism is the largest for A_2B_3 micellar solution, Table 2). By the end of the second stage, the number-average aggregation number equilibrates, which indicates that the number of aggregates becomes stable. During the third stage the weight-average aggregation number continues to increase very slowly due to the adjustment of the aggregation number distribution. The weight-average aggregation number distribution, which still exhibits a bimodal shape in the earlier times of the final stage of micellization, gradually becomes unimodal with the peak position corresponding to the final equilibrium aggregation number (Figure 7). Statistical analysis of different events occurring during stage three shows that exchange of unimers and small aggregates with micelles becomes more dominant and the probability of micelle fission/fusion declines, although the contribution of micelle fusion to the overall chain redistribution remains significant as these multioligomer events are rather effective.

The boundaries between different stages and the relative contribution of different kinetic processes to micellization depend on the system properties, such as the interaction energy between blocks and solvent, polymer concentration, block length, etc. We found that increasing the polymer concentration speeds up not only the initial stage of unimer coupling, but also the whole micellization process due to an increase of the probability (and contribution) of micelle fusion/fission events. An increase the hydrophobic interaction energy a_{AB} dramatically slows down the micellization process: while micelle growth at early times follows nearly the same pathway independent of the interaction energy, more events are required to achieve the larger final equilibrium aggregation number and there is a higher potential barrier for unimer expulsion or micelle fission. With an increase in the interaction energy, the relative frequency of occurrence and contribution of unimer exchange to the micellization process generally increases, contribution of processes involving small aggregates decreases, while micelle fusion/fission remains practically unaffected. Comparing the process of micelle self-assembly from unimers for A_4B_x and A_2B_3 solutions, we found that the overall micellization process for A_4B_x solution proceeds via the same stages, but the time windows for the different stages noticeably expand with an increase of oligomer length. We have also investigated the effect of increasing the hydrophilic block length and found that while the overall number of kinetic events decreases, the relative frequencies and contributions of different kinetic processes remain practically unaffected. The first two stages of micellization take longer time for oligomers with a longer hydrophilic block, while the ratio of reactants in aggregate addition reactions P_a/P_b increases.

In conclusion, our simulation results show that the contribution of micelle fusion to micellization remain substantial from the beginning to the end of the micellization process and is responsible for the observed bimodal distribution at intermediate stages of micellization. Besides unimer exchange and micelle fusion/fission, the processes involving small aggregates play an important role (with a contribution of about 20% to all chain exchange) and need to be taken into account while analyzing the kinetics of micelle formation.

Acknowledgment. We are grateful to Dr. Hadrian Djohari for useful discussions regarding DPD technique. This material is based upon work supported by the National Science Foundation under Grant No. 0348302. All simulations were conducted on the High Performance Computing cluster of Case Western Reserve University.

Supporting Information Available: Text discussing the deterimination of the cmc, aggregation number distribution, micelle structure, micellization kinetics data and diffusion coefficients for A_4B_x chains including figures showing plots of volume fractions, aggregation number distribution, monomer density profiles, time evolution of the aggregation number, and average aggregation number during micellization and tables of events and fractions of chains exchanged and diffusion coefficients. This material is available free of charge via the Internet at http://pubs.acs.org.

References and Notes

(1) Riess, G. *Prog. Polym. Sci.* **2003**, *28*, 1107.
(2) Gohy, J. F. *Adv. Polym. Sci.* **2005**, *190*, 65.
(3) Zana, R. *Dynamics of surfactant self-assemblies: micelles, microemulsions, vesicles, and lyotropic phases*; CRC Press: Boca Raton, FL, 2005.
(4) (a) Honda, C.; Hasegawa, Y.; Hirunuma, R.; Nose, T. *Macromolecules* **1994**, *27*, 7660. (b) Honda, C.; Abe, Y.; Nose, T. *Macromolecules* **1996**, *29*, 6778.
(5) Wang, Y.; Kausch, C. M.; Chun, M.; Quirk, R. P.; Mattice, W. L. *Macromolecules* **1995**, *28*, 904.
(6) Johnson, B. K.; Prud'homme, R. K. *Phys. Rev. Lett.* **2003**, *91*, 118302.
(7) Zhu, Z.; Armes, S. P.; Liu, S. *Macromolecules* **2005**, *38*, 9803.
(8) (a) Lund, R.; Willner, L.; Richter, D.; Dormidontova, E. E. *Macromolecules* **2006**, *39*, 4566. (b) Lund, R.; Willner, L.; Stellbrink, J.; Lindner, P.; Richter, D. *Phys. Rev. Lett.* **2006**, *96*, 68302.
(9) Zhu, Z.; Xu, J.; Zhou, Y.; Jiang, X.; Armes, S. P.; Liu, S. *Macromolecules* **2007**, *40*, 6393.
(10) Zhang, J.; Xu, J.; Liu, S. *J. Phys. Chem. B.* **2008**, *112*, 11284.
(11) Rao, J.; Zhang, J.; Xu, J.; Liu, S. *J. Colloid Interface Sci.* **2008**, *328*, 196.
(12) Rao, J.; Xu, J.; Luo, S.; Liu, S. *Langmuir* **2007**, *23*, 11857.
(13) Lund, R.; Willner, L.; Monkenbusch, M.; Panine, P.; Narayanan, T.; Colmenero, J.; Richter, D. *Phys. Rev. Lett.* **2009**, *102*, 188301.
(14) (a) Aniansson, E.; Wall, S. *J. Phys. Chem.* **1974**, *78*, 1024. (b) Aniansson, E.; Wall, S. *J. Phys. Chem.* **1975**, *79*, 857. (c) Aniansson, E.; Wall, S.; Almgren, M.; Hoffmann, H.; Kielmann, I.; Ulbricht, W.; Zana, R.; Lang, J.; Tondre, C. *J. Phys. Chem.* **1976**, *80*, 905.
(15) (a) Lessner, E.; Teubner, M.; Kahlweit, M. *J. Phys. Chem.* **1981**, *85*, 1529. (b) Lessner, E.; Teubner, M.; Kahlweit, M. *J. Phys. Chem.* **1981**, *85*, 3167. (c) Kahlweit, M. *J. Colloid Interface Sci.* **1982**, *90*, 92.
(16) Halperin, A.; Alexander, S. *Macromolecules* **1989**, *22*, 2403.
(17) Dormidontova, E. E. *Macromolecules* **1999**, *32*, 7630.
(18) Kuni, F.; Rusanov, A.; Shchekin, A.; Grinin, A. *Russ. J. Phys. Chem.* **2005**, *79*, 833.
(19) Nyrkova, I. A.; Semenov, A. N. *Macromol. Theory Simul.* **2005**, *14*, 569.
(20) Rodrigues, K.; Mattice, W. L. *J. Chem. Phys.* **1991**, *94*, 761.
(21) Wang, Y.; Mattice, W.; Napper, D. *Langmuir* **1993**, *9*, 66.
(22) Pepin, M.; Whitmore, M. *Macromolecules* **2000**, *33*, 8654.
(23) Marrink, S.; Tieleman, D.; Mark, A. *J. Phys. Chem. B* **2000**, *104*, 12165.
(24) Chen, T.; Hynninen, A. P.; Prud'homme, R. K.; Kevrekidis, I. G.; Panagiotopoulos, A. Z. *J. Phys. Chem. B* **2008**, *112*, 16357.
(25) (a) Hoogerbrugge, P.; Koelman, J. M. V. A. *Europhys. Lett.* **1992**, *19*, 155. (b) Koelman, J. M. V. A.; Hoogerbrugge, P. *Europhys. Lett.* **1993**, *21*, 363.
(26) Groot, R. D.; Warren, P. B. *J. Chem. Phys.* **1997**, *107*, 4423.
(27) Jiang, W.; Huang, J.; Wang, Y.; Laradji, M. *J. Chem. Phys.* **2007**, *126*, 044901.
(28) (a) Groot, R. D.; Madden, T. J. *J. Chem. Phys.* **1998**, *108*, 8713. (b) Groot, R. D. *Langmuir* **2000**, *16*, 7493.
(29) Jury, S.; Bladon, P.; Cates, M.; Krishna, S.; Hagen, M.; Ruddock, N.; Warren, P. *Phys. Chem. Chem. Phys.* **1999**, *1*, 2051.
(30) Xia, J.; Zhong, C. *Macromol. Rapid Commun.* **2006**, *27*, 1110.
(31) Ortiz, V.; Nielsen, S. O.; Discher, D. E.; Klein, M. L.; Lipowsky, R.; Shillcock, J. *J. Phys. Chem. B* **2005**, *109*, 17708.
(32) Schlijper, A.; Hoogerbrugge, P.; Manke, C. *J. Rheol.* **1995**, *39*, 567.
(33) Spenley, N. *Europhy. Lett.* **2000**, *49*, 534.
(34) Sheng, Y. J.; Wang, T. Y.; Chen, W. M.; Tsao, H. K. *J. Phys. Chem. B* **2007**, *111*, 10938.
(35) Allen, M.; Tildesley, D. *Computer simulation of liquids*: Oxford University Press: New York, 1990.
(36) Plimpton, S. *J. Comput. Phys.* **1995**, *117*, 1.
(37) Humphrey, W.; Dalke, A.; Schulten, K. *J. Mol. Graphics* **1996**, *14*, 33.
(38) Ruckenstein, E. N., R.; Nagarajan, R. *J. Phys. Chem.* **1975**, *79*, 2622.
(39) Floriano, M. A.; Caponetti, E.; Panagiotopoulos, A. Z. *Langmuir* **1999**, *15*, 3143.
(40) Milchev, A.; Bhattacharya, A.; Binder, K. *Macromolecules* **2001**, *34*, 1881.
(41) Kenward, M.; Whitmore, M. *J. Chem. Phys.* **2002**, *116*, 3455.
(42) Viduna, D.; Milchev, A.; Binder, K. *Macromol. Theory Simul.* **1998**, *7*, 649.
(43) Nagarajan, R.; Ganesh, K. *J. Chem. Phys.* **1989**, *90*, 5843.
(44) Willner, L.; Poppe, A.; Allgaier, J.; Monkenbusch, M.; Lindner, P.; Richter, D. *Europhy. Lett.* **2000**, *51*, 628.
(45) Haliloglu, T.; Bahar, I.; Erman, B.; Mattice, W. L. *Macromolecules* **1996**, *29*, 4764.